RM E53F02

NACA RM E53F02

6823

TECH LIBRARY KAFB, NM
0144403

# RESEARCH MEMORANDUM

## PRELIMINARY RESULTS OF HEAT TRANSFER FROM A STATIONARY AND ROTATING ELLIPSOIDAL SPINNER

By U. von Glahn

Lewis Flight Propulsion Laboratory
Cleveland, Ohio

AFMDC
TECHNICAL LIBRARY
AFL 2811

NATIONAL ADVISORY COMMITTEE
FOR AERONAUTICS

WASHINGTON
August 6, 1953

TECH LIBRARY KAFB, NM
0143403



NATIONAL ADVISORY COMMITTEE FOR AERONAUTICS

RESEARCH MEMORANDUM

# PRELIMINARY RESULTS OF HEAT TRANSFER FROM A STATIONARY AND ROTATING ELLIPSOIDAL SPINNER

By U. von Glahn

9062

## SUMMARY

Convective heat-transfer coefficients in dry air were obtained for an ellipsoidal spinner of 30-inch maximum diameter for both stationary and rotating operation over a range of conditions including airspeeds up to 275 miles per hour, rotational speeds up to 1200 rpm, and angles of attack of zero and 4°. The results are presented in terms of Nusselt numbers, Reynolds numbers, and convective heat-transfer coefficients. The studies included both uniform heating densities over the spinner and uniform surface temperatures.

In general, the results showed that rotation will increase the convective heat transfer from a spinner, especially in the turbulent-flow regions. Rotation of the spinner at 1200 rpm and at a free-stream velocity of 275 miles per hour increased the Nusselt number parameter in the turbulent-flow region by 32 percent over that obtained with a stationary spinner; whereas in the nose region, where the flow was laminar, an increase of only 18 percent was observed. Transition from laminar to turbulent flow occurred over a large range of Reynolds numbers primarily because of surface roughness of the spinner. Operation at an angle of attack of 4° had only small effects on the local convective heat transfer for the model studied.

CK-1

## INTRODUCTION

In the determination of minimum thermal-icing-protection requirements for turbojet-powered all-weather aircraft, a knowledge of heat transfer from stationary streamlined bodies of revolution is required to evaluate more closely the heat demand for such components as engine accessory housings and radomes (ref. 1). Icing of the radome may cause deterioration of radar transmission, while icing of the engine accessory housing may cause pressure losses at the compressor face resulting in a loss in engine thrust. In addition, the development of large turbine-propeller engines using large-diameter geared propellers requires icing protection for the propeller spinner. Icing of the spinner may reduce the pressure recovery available in air intakes located downstream from

the spinner, thereby causing a loss in engine thrust and power. The uncontrolled throw-off of large ice formations from the spinner may also cause structural damage to propeller-blade cuffs and aircraft and engine components located downstream of the spinner. In addition, asymmetrical uncontrolled shedding of ice formations from a spinner may produce undesirable unbalance causing excessive vibration of the propeller-spinner configuration.

Limited data are available on average and local heat-transfer coefficients for spheres (refs. 2 to 6), while little information exists on heat transfer from simple bodies of revolution. Information that is available does not appear to be directly applicable to the icing problems concerning high-speed aircraft and also does not consider the effect of body rotation on heat transfer.

As part of a general program to determine icing and icing protection of bodies of revolution, a study was made at the NACA Lewis laboratory to determine the external convective heat transfer obtained from an ellipsoidal spinner which incorporated an internal electric heater. Data were obtained with and without rotation of the spinner at dry-air conditions over a range of airspeeds up to 275 miles per hour and rotational speeds up to 1200 rpm. The study presented herein is necessarily restricted because of failure of the heaters prior to completion of the program; hence, no data in icing conditions were obtained.

## SYMBOLS

The following symbols are used in this report:

| | |
|---|---|
| $h$ | convective heat-transfer coefficient, Btu/(hr)(sq ft)($^{\circ}$F) |
| $k$ | thermal conductivity of air, Btu/(hr)(sq ft)($^{\circ}$F/ft) |
| Nu | Nusselt number, dimensionless, based on local surface distance and free-stream air thermal conductivity except as noted |
| $n$ | rotational speed, rps |
| Pr | Prandtl number, dimensionless, based on free-stream air properties of viscosity and conductivity |
| $q_i$ | internal rate of heat-flow loss, Btu/(hr)(sq ft) |
| $q_t$ | total rate of heat-flow input, Btu/(hr)(sq ft) |

2906

CK-1 back 9062

Re Reynolds number, dimensionless, based on local surface distance, local air velocity, and free-stream air properties of density and viscosity except as noted

r local spinner radius, ft

$t_d$ datum temperature, $^{\circ}F$

$t_i$ temperature of neoprene insulation, $^{\circ}F$

$t_s$ surface temperature, $^{\circ}F$

V local resultant velocity of spinner, ft/sec

$V_r$ local component of V in a plane perpendicular to spinner axis of rotation, $2\pi rn$, ft/sec

$V_t$ local streamwise velocity just outside of boundary layer, ft/sec

$\delta$ boundary-layer thickness, ft

Subscripts:

D parameter based on equivalent sphere diameter and free-stream velocity

$l$ parameter based on local air properties of density, conductivity, and viscosity

s spinner surface

1 heater side of neoprene insulation

2 model interior side of neoprene insulation

## DESCRIPTION OF APPARATUS

The spinner model, an ellipsoidal shape with a major axis of 37.5 inches and a minor axis of 15 inches, was mounted on a faired afterbody in the 6- by 9-foot test section of the icing-research tunnel (fig. 1). The spinner model was fabricated of 0.062-inch aluminum, spun to the required shape. The spinner contour is shown in figure 2 together with a table of the spinner coordinates. Heat was supplied to the spinner by means of six electric heating pads; the surface area heated by each pad and the maximum allowable heating density are shown in table I.

Construction details of the electrically heated spinner also are shown in figure 2. The heaters consisted of 30-gage Nichrome heating wires spaced 0.125 inch on centers. The heater wires were encased between two plies of glass cloth, each 0.006 inch thick. The heater wires and cloth were in turn sandwiched between two layers of neoprene, each 0.010 inch thick. The inner side of the heater (fig. 2) included an additional neoprene insulation ply of 0.060-inch thickness. Each of the six heating pads shown in figure 2 was connected to a separate variable autotransformer which permitted selective control of heat input and axial-heat distribution. The total power input to each heating pad was measured by a recording wattmeter.

2906

The model was instrumented to obtain the heat dissipation from the heaters to the inside of the spinner shell as well as the surface temperatures. The surface thermocouples were spaced at 1-inch intervals measured from the spinner nose for heating elements A, B, and C (fig. 2). For heating elements D and E the thermocouple spacing was 1.5 inches while for heating element F the spacing was increased to 3 inches. In the middle of each heatable section, thermocouples were located in three layers as shown in figure 2. The two sets of thermocouples on the 0.060-inch neoprene insulation were used to obtain the heat loss to the spinner interior. All thermocouples consisted of 30-gage iron and constantan wire. The surface thermocouples were peened into the aluminum shell of the spinner, while the thermocouples on the neoprene insulation were connected to 0.25-inch-diameter brass disks which were cemented to the neoprene. The brass disks were used to provide an average heater-insulation temperature rather than the temperature over or between heater wires.

The means used to transmit the temperatures from the thermocouples to the recorder is shown schematically in figure 3. All the thermocouple leads from the spinner were fed through a hollow motor shaft to the rear of the motor housing and through a thermocouple selector switch into a steam-filled jacket that rotated with the shaft. From the rotating jacket, copper leads were attached to a slip-ring and brush assembly. From this assembly, copper leads were again led into a steam-filled stationary jacket. Iron-constantan leads were used from the stationary jacket to a thermocouple selector unit and to a flight recorder. The steam jacket was used to provide a constant temperature at critical junctions in the thermocouple, circuiting when the wire metals in the thermocouple leads were changed from iron and constantan to copper and back again.

A 7.5-horsepower electric variable-speed motor was used to drive the spinner for the rotating phase of the program. A "power pineapple" assembly, consisting of seven sets of copper slip rings and copper brushes rated at 45 amperes and two sets of rings and brushes rated at 3 amperes, was mounted around the motor shaft between the spinner and the motor.

This assembly was used to supply electric power selectively to the heating pads.

A small container for an ice bath and a thermocouple was mounted on the bulkhead at the base of the spinner. The temperature of the ice bath (32° F) was transmitted by means of the thermocouple through the entire temperature-measuring system to the flight recorder; a means was thereby provided to determine any errors in absolute temperature measurement that might occur due to malfunctioning of the steam jackets or wear of the slip-ring assembly.

2906

The pressure distribution over the spinner surface was obtained by means of pressure belts cemented to the spinner surface.

Free-stream temperature conditions were measured by means of shielded thermocouples from which the approximate air total temperature was recorded on independent recorders. Rotational speeds were determined by using a stroboscopic lighting system consisting of a single flash lamp synchronized with the spinner.

## PROCEDURE AND TECHNIQUES

The pressure distribution over the spinner was obtained only for stationary operation of the model. Data were obtained in both horizontal and vertical planes at a spinner angle of attack of zero and in a vertical plane at a spinner angle of attack of 4°.

Heat-transfer data were primarily obtained by using a uniform total heat input to the entire heatable area of the spinner. Power density values of 3, 4, and 5 watts per square inch were studied. Additional limited studies were made for a uniform surface-temperature distribution within the limits of the heater configuration. Data were recorded only after sufficient time had elapsed to insure that the temperature had stabilized. In general, all heat-transfer studies were made at a total air temperature of 0° F.

Prior to each day's testing, a check was made by means of the ice bath at the spinner base to determine whether the temperature-measuring system was functioning properly.

The spinner model was studied in dry air over the following nominal range of operating conditions:

| Airspeed, mph | Angle of attack, deg | Rotational speed, rpm |
|---|---|---|
| 175 | 0 | 0, 800, 1200 |
| 175 | 4 | 0 |
| 275 | 0 | 0, 1200 |
| 275 | 4 | 0 |

2906

From measurements made in reference 7 of the effective thermal resistance of a layer of neoprene between two layers of thermocouples, an average thermal conductivity of 107.4 Btu/(hr)(sq ft)($^{o}$F) was obtained for a sheet of neoprene 0.012 inch thick. This value of thermal conductivity, adjusted for the additional thickness of neoprene in the spinner, was used with the measured temperature drop to calculate the internal heat loss from the heaters. Conduction effects in the heater and metal spinner shell were neglected in all calculations of heat-transfer.

## RESULTS AND DISCUSSION

### Velocity Distribution

An evaluation of local convective heat-transfer data from a body of revolution requires that the local velocity over the surface be known. The results of a pressure-distribution study from which the local velocities $V_t$ over the nonrotating spinner were obtained are shown in figure 4(a) for zero angle of attack and airspeeds of 175 and 275 miles per hour, respectively. The experimental values, uncorrected for tunnel effects, are only slightly higher than those obtained analytically by means of reference 8 for a prolate spheroid of the same axes dimensions as the spinner. No effort was made to correct the experimental values for tunnel effects inasmuch as the analysis of experimental heat-transfer data requires the use of the actual measured local velocity values. The velocity distribution over the nonrotating spinner at an angle of attack of 4$^{o}$ is shown in figure 4(b); the distribution does not differ appreciably from the values obtained at zero because of the rather blunt physical characteristics of the spinner which caused only small flow changes around the spinner at low angles of attack.

With spinner rotation, no direct measurements of local velocity were obtained; however, the local resultant velocity was calculated conventionally from the local tangential and rotational velocities as

$$V = \sqrt{V_t^2 + V_r^2} \tag{1}$$

The local resultant velocities thus obtained were used in all calculations of heat transfer for the case of the rotating spinner presented in subsequent sections of this report.

2906

## Heat-Transfer Analysis

Internal heat loss. - The loss through the heater to the model interior was obtained by a measurement of the heat transfer through the instrumented neoprene insulation by the following relation:

$$q_i = 21.5(t_{i,1} - t_{i,2}) \text{ Btu/(hr)(sq ft)} \tag{2}$$

The constant 21.5 was obtained by means of reference 7.

A compilation of all the heat losses through the 0.060-inch neoprene insulation is presented in table II. These data were cross-plotted and extrapolated to obtain estimated heat losses for tests from which direct temperature measurements through the 0.060-inch neoprene insulation were unobtainable. The average heat loss to the model interior for stationary operation of the spinner amounted to about 14.1 percent for the nose-section heater and to about 6.3 percent for the rearmost heater. For the rotating spinner, the average heat loss at the nose-section heater was similar to the stationary spinner; however, the loss increased for the two rearmost heaters, with the rearmost heater losing about 10.0 percent to the model interior. The increased heat loss for the rearward heaters appears to have been caused by an increase in heat transfer to the spinner mounting structure; the heat-transfer increase was a result of the increased air circulation through the model caused by spinning. Uncertainties in the measurement of the internal heat losses may have contributed an error of ±5 percent to the calculation of the external heat-transfer rates.

External convective heat transfer. - The external convective heat-transfer coefficients at each heater were calculated from the measured total heat input, external-surface temperature, unheated-surface or datum temperature, and internal heat loss by the following relation:

$$h = \left(\frac{q_t - q_i}{t_s - t_d}\right) \tag{3}$$

In order to simplify calculation of the Nusselt and Reynolds number heat-transfer parameters, especially in the case of the rotating spinner, the

air properties were evaluated generally at free-stream values of density, viscosity, and conductivity; however, local values of velocity were used in all cases. In order to indicate the effect on the heat-transfer parameters contributed by the use of local values of density, viscosity, and conductivity, several calculations for nonrotation of the spinner based on these local values also are included and discussed briefly in the section Heat-Transfer Results.

The datum temperatures $t_d$ were obtained from surface-temperature measurements with no heat applied to the spinner and were related to the free-stream total air temperature. A discrepancy between the flight recorder for the total air-temperature measurements and the recorder for the surface-temperature measurements caused an inaccuracy of $\pm 3^{\circ}$ F in the determination of the datum-temperature level.

2906

It is of interest to compare the experimental values of heat transfer from the nose region of the stationary spinner with heat-transfer values determined for spheres from the aft regions of the spinner and with flat-plate values; the comparison is made in a manner similar to that for making analysis of airfoils with cylinders and flat plates. Theoretical calculations of the laminar boundary-layer thickness for a sphere were made in reference 9 and were used to determine local heat-transfer coefficients about a sphere (ref. 6) by the relation

$$\frac{h\delta}{k} = 0.765 \tag{4}$$

Although the spinner is in a 3-dimensional flow field compared with a 2-dimensional flow field for a flat plate, the comparison may be considered somewhat valid for the aft portions of the spinner because of the large radius of curvature of the spinner in the direction of the air streamlines. For this comparison, the following analytical expression for flat-plate turbulent flow given in reference 10 was used:

$$Nu = 0.0296\ Pr^{1/3}\ Re_s^{0.8} \tag{5}$$

## Heat-Transfer Results

Nonrotating spinner with uniform heat density. - The heat-transfer data for stationary operation of the spinner at a zero angle of attack are presented in terms of the nondimensional Nusselt number, Prandtl number, and Reynolds number in figure 5. These data are evaluated in terms of a distance parameter based on the surface distance measured from the stagnation point. In addition to the experimental data, theoretical and experimental values for a sphere by means of references 9 and 6, respectively, and analytical values for turbulent flow

over a flat plate (eq. (5)) have been included in this figure. The curves for the sphere values are based on a sphere diameter of 15 inches, a size which was determined to have approximately the same pressure distribution as the initial 4 to 5 inches in the nose region of the spinner. It was believed, consequently, that the laminar boundary-layer development for the spinner and sphere should be similar; hence, the heat-transfer characteristics should also be very similar. In the region of $Re_s < 5 \times 10^5$, the experimental spinner data lie considerably higher than but approximately parallel to the sphere values. The results are in general agreement with the order of magnitude of the airfoil data of reference 10. The laminar Nusselt number parameter values of the nose region are approximately 70 percent higher than the theoretical sphere values calculated by means of reference 9 (Pr = 1.0) and 30 percent higher than the experimental values reported in reference 6. A comparison of the Nusselt numbers at the stagnation point for the spinner and spheres is shown in figure 6 as a function of Reynolds number. The stagnation-point heat transfer for the spinner is shown to be of the same order of magnitude as the results obtained from references 5, 6, and 9. The spinner Nusselt number values at the stagnation point lie approximately 57 percent higher than sphere values based on reference 9 and 37 percent higher than sphere data extrapolated from the experimental studies of reference 6. It should be noted that the results based on reference 9 were obtained from equation 4 and are based on a Prandtl number of 1.0; consequently, these values should be approximately 10 percent greater for the normal range of Prandtl number for air.

The increase in heat-transfer values in the laminar nose region with reference to the calculated laminar-flow sphere values (fig. 5) is believed to be caused, in large part, by the turbulence level of the tunnel air stream. Similar increases in heat transfer over cylinders have been reported in references 3 and 11 and were caused by turbulence in the air stream and by model roughness. A full turbulent-flow condition was reached at a Reynolds number of approximately $6 \times 10^6$. In the case of turbulent flow, the experimental heat-transfer Nusselt number agrees closely with the turbulent-flow flat-plate values from equation (5) (fig. 5).

A wide variation of curves in the transition region occurred as the studies progressed because of the increased roughness of the spinner surface caused by dirt and rust particles in the tunnel air stream. The initial tests indicated a steep slope for the transition curve, with transition starting at a Reynolds number of about $1.5 \times 10^6$. Progressive roughening of the surface moved the transition forward as shown by a comparison of the curves at 175 miles per hour for a heat input of 4 watts per square inch (fig. 5, square and diamond symbols); the curve showing delayed transition (square symbols) was attained with a smooth surface while the curve showing early transition (diamond symbols) was obtained with a roughened surface. The curves at 275 miles per hour

2906 CK-2

(fig. 5) were obtained with approximately the same degree of surface roughness and indicate that an increase in heat density from 3 to 5 watts per square inch tends to delay transition slightly as the total heat input per unit area is increased. The earliest transition appeared to start at a Reynolds number of about $6 \times 10^5$ and occurred with a heating density of 3 watts per square inch at 275 miles per hour. A portion of this movement of the transition curve may be attributed to the accuracy with which the heat-transfer rates were calculated. With the lower heat densities, an error of $\pm 3^\circ$ in the datum temperature will amount to an error of as much as ±15 percent in the transition-region Nusselt number because of the low level of the temperature rise; with a high heat density (high surface temperatures), the same error in temperature would amount to only ±5 percent in the Nusselt number.

For comparative purposes with figure 5 and data from reference 10, two of the stationary spinner studies were analyzed with the use of local values of the air properties (density, viscosity, and conductivity) based on local surface temperatures for the Nusselt and Reynolds number parameters as shown in figure 7. The resulting curves are quite similar to those shown in figure 5, being displaced somewhat to the left of the original curves in the transition region. No improvement in the data scatter can be discerned. A comparison of the Nusselt parameter based on local conditions at the spinner surface with typical results from reference 10 for a symmetrical NACA 65,2-016 airfoil and values for turbulent flow over a flat plate are also shown in figure 7. It can be seen from this comparison that the data, in most respects, are quite similar.

Rotating spinner with uniform heat density. - In general, the variation of Nusselt number with Reynolds number for a rotating spinner (fig. 8) shows the same characteristics as the values for the stationary spinner; however, for the same Reynolds number the Nusselt number is somewhat higher. Both the Nusselt number and the Reynolds number are based on a graphically determined helical-surface distance associated with the rotational speeds used for the spinner. The increase in Nusselt number resulted from a change in boundary-layer characteristics caused, in part, by the rotational velocity component of the boundary layer which causes a twisting shear in the boundary layer as well as possible changes in the boundary-layer profile from small centrifugal effects. A comparison of figures 8(a) and (b) with the nonrotating data shown in figure 5 indicates that the Nusselt number is increased by about 11 and 18 percent in the laminar region for rotational speeds of 800 and 1200, respectively; while in the turbulent region, the Nusselt number is increased by about 7 and 32 percent, respectively, for these two rotational speeds. These percentage increases may be varied somewhat by refairing the curves through the scattered data.

2906

Transition for the rotating spinner begins at a Reynolds number of about $1 \times 10^6$ and reaches full turbulent flow at about $4.8 \times 10^6$. There is no apparent difference in transition for the two rotational speeds studied other than a shift in the level of Nusselt number. An increase in the heating density from 3 to 4 watts per square inch caused a slight delay in transition, as was the case for the nonrotating spinner, at an air velocity of 275 miles per hour. Although the higher-speed data (275 mph) lie slightly above the 175-mile-per-hour data, this shift is believed to be caused primarily by the previously discussed inaccuracy in datum-temperature values. The slopes for the transition curves are similar for both rotating and nonrotating operation of the spinner.

9062

CK-2 back

Convective heat-transfer coefficients with uniform heating rate. - The local external heat-transfer coefficient and local surface-temperature rise are shown in figure 9 as a function of surface distance for both stationary and rotating operation of the spinner. These values of heat-transfer coefficients were obtained for uniform total heat densities of 3, 4, and 5 watts per square inch and for airspeeds of 175 and 275 miles per hour. For stationary operation the external heat-transfer coefficient in the nose region of the spinner at the lower airspeed was approximately 14 Btu/(hr)(sq ft)($^\circ$F), while at the higher airspeed the coefficient increased to approximately 18.5 Btu/(hr)(sq ft)($^\circ$F). With a spinner rotation of 1200 rpm, the heat-transfer coefficient in the nose region increased to approximately 15 and 21 Btu/(hr)(sq ft)($^\circ$F) for airspeeds of 175 and 275 miles per hour, respectively. At a rotational speed of 800 rpm and 175 miles per hour, the heat-transfer coefficient was about 14.5 Btu/(hr)(sq ft)($^\circ$F) at the nose region. In the turbulent-flow region near the aft end of the spinner, the heat-transfer coefficient for the stationary spinner was approximately 29 and 45 Btu/(hr)(sq ft)($^\circ$F) for airspeeds of 175 and 275 miles per hour, respectively. Rotation of the spinner increased the turbulent heat-transfer coefficient (air velocity, 175 mph) in proportion to the rotational speed; at 800 rpm the coefficient increased to approximately 35 Btu/(hr)(sq ft)($^\circ$F), while at 1200 rpm the coefficient increased to about 39 Btu/(hr)(sq ft)($^\circ$F).

Convective heat-transfer coefficients with uniform surface temperature. - Heat-transfer coefficients obtained with an approximately uniform surface temperature are shown in figure 10 for stationary and rotating operation of the spinner. The data, in general, are of the same magnitude as those obtained with a uniform heating rate and nonuniform surface temperature. Only in the transition region do the heat-transfer coefficients differ materially; the data show that with a uniform surface temperature the slope of the transition curve becomes steeper than that obtained with a nonuniform surface temperature. The difference in the apparent change in heat-transfer coefficients in the transition region may result from the neglect of conduction which will affect the surface temperatures and hence the analysis of the data. The heat-transfer-coefficient differences between stationary and rotating operation of the

spinner with a uniform surface temperature were similar to those obtained with nonuniform surface temperatures (uniform heating rate).

Heat transfer at angle of attack of 4°. - The convective heat-transfer coefficients and surface temperatures obtained with uniform total heat inputs are shown in figure 11 for the stationary spinner at an angle of attack of 4° and airspeeds of 175 and 275 miles per hour, respectively. These data were obtained in the normally vertical plane of the spinner and are the maximum and minimum heat-transfer coefficients axially along the spinner surface. Because the spinner studied was a rather blunt specimen, an angle of attack of 4° did not greatly influence the flow field about the spinner, as indicated previously by the pressure distribution about the spinner (fig. 4(b)); hence, the convective heat-transfer coefficients at an angle of attack of 4° did not change appreciably from those at zero. A more rapid approach of transition was observed on the upper surface than on the lower surface because of surface roughness at the spinner nose region.

2906

Application of data to icing conditions. - Ⓐ The dry-air heat-transfer data obtained for the spinner may be used in the calculation of the approximate heating requirements for ice prevention in icing conditions by observing the general results of heat transfer from an airfoil in icing conditions given in reference 10. The data obtained in reference 10 for a symmetrical NACA 65,2-016 airfoil indicate a consistent trend for transition in icing conditions to begin near the limit of impingement. The slope of the Nusselt parameter curve in the transition region in icing conditions (for both tunnel and flight tests) is generally quite similar to the slope obtained in dry air with a rough model surface; however, a slight tendency exists for the slope to be less steep.

The impingement characteristics for bodies of revolution may be estimated from computed droplet trajectories such as reported in reference 12. It should be noted that consideration of cloud-droplet-size distribution is of primary importance in the determination of the weight rate of water impingement on large bodies of revolution. This factor has been adequately demonstrated by experimental studies in the NACA Lewis icing-research tunnel, also reported in reference 12.

The requirements for a thermal icing-protection system based on the tunnel results in the laminar boundary-layer region will be conservative as indicated by a consideration of the heat balance equation in icing conditions. The conservatism is caused by the higher convective heat-transfer coefficients obtained in the tunnel compared with theoretical and flight data (ref. 10). The amount by which the heat requirements are conservative cannot be evaluated directly because it is dependent on the specific conditions at which the body is to be operated. For bodies in which the laminar boundary-layer extent is small compared with the total thermally protected area, the heating requirements based on heat-transfer coefficients obtained in the tunnel will be only slightly conservative.

2906

## SUMMARY OF RESULTS

From a study of the convective heat transfer in dry air from an ellipsoidal spinner for both stationary and rotating operation the following results were obtained:

1. Rotation of the spinner at 1200 rpm and at a free-stream velocity of 275 miles per hour increased the Nusselt number parameter in the turbulent-flow region by approximately 32 percent over values obtained with a stationary spinner. In the spinner-nose region, the Nusselt number parameter increased by about 18 percent because of rotation at similar operating conditions.

2. The transition from laminar to turbulent flow occurred over a range of Reynolds numbers which depended on the air velocity and the surface roughness of the spinner model. In general, with the surface roughened by dirt and tunnel rust particles, transition began at a Reynolds number in the range of about $6\times10^5$ to $1\times10^6$ and ended at about $6\times10^6$ for the stationary spinner.

3. Rotation of the spinner caused full turbulent flow to be reached at a lower Reynolds number ($4.8\times10^6$) than for stationary operation of the spinner.

4. Operation at an angle of attack of $4^\circ$ had only small local effects on the convective heat-transfer coefficients for the stationary spinner.

5. The heat-transfer data obtained were in the same general orders of magnitude as the data obtained in a previous study of a symmetrical NACA 65,2-016 airfoil (ref. 10).

Lewis Flight Propulsion Laboratory
National Advisory Committee for Aeronautics
Cleveland, Ohio, May 19, 1953

## REFERENCES

1. Lewis, James P.: An Analytical Study of Heat Requirements for Icing Protection of Radomes. NACA RM E53A22, 1953.

2. McAdams, William J.: Heat Transmission. Second ed., McGraw-Hill Book Co., Inc., 1942.

3. Jakob, Max: Heat Transfer. Vol. I. John Wiley & Sons, Inc., 1949.

4. Ingebo, Robert D.: Vaporization Rates and Heat-Transfer Coefficients for Pure Liquid Drops. NACA TN 2368, 1951.

5. Frössling, Nils: Verdunstung Wärmeübergang und Geschwindigkeitsverteilung bei Zweidimensionaler und rotationssymmetrischer Laminaer Grenzschichtströmung. Lunds Universitates Arsshrift, Bd. 36, Nr. 4, 1940.

6. Cary, John R.: The Determination of Local Forced Convection Coefficients for Spheres. Eng. Rep. LB-16507, Douglas Aircraft Co., Inc., May 23, 1952.

7. Lewis, James P., and Bowden, Dean T.: Preliminary Investigation of Cyclic De-Icing of an Airfoil Using an External Electric Heater. NACA RM E51J30, 1952.

8. Zahm, A. F.: Flow and Drag Formulas for Simple Quadrics. NACA Rep. 253, 1927.

9. Tomotika, S.: The Laminar Boundary Layer on the Surface of a Sphere in a Uniform Stream. R.& M. No. 1678, British A.R.C., 1936.

10. Gelder, Thomas F., and Lewis, James P.: Comparison of Heat Transfer from Airfoil in Natural and Simulated Icing Conditions. NACA TN 2480, 1951.

11. Giedt, W. H.: Effect of Turbulence Level of Incident Air Stream on Local Heat Transfer and Skin Friction on a Cylinder. Jour. Aero. Sci., vol. 18, no. 11, Nov. 1951, pp. 725-730.

12. Lenherr, F. E., and Young, R. W.: Computation of Water Catch on Axial Symmetric Aircraft Radomes. TDM-77, Northrop Aircraft, Inc., Dec. 17, 1952. (Prog. Rep. III, AF 33(038)-1817.)

2906

2906

TABLE I. - SPINNER HEATER CHARACTERISTICS

| Heater element | Area, sq in. | Maximum power-density rating, w/sq in. |
|---|---|---|
| A | 32 | 10 |
| B | 124 | 10 |
| C | 193 | 8 |
| D | 360 | 8 |
| E | 785 | 6 |
| F | 1260 | 6 |

TABLE II. - INTERNAL HEAT LOSS THROUGH HEATER FOR UNIFORM HEAT DENSITIES AND ZERO ANGLE OF ATTACK

| Air velocity, mph | 175 | | 175 | | 275 | | 275 | | 275 | |
|---|---|---|---|---|---|---|---|---|---|---|
| Power density, w/sq in. | 3 | | 4 | | 3 | | 4 | | 5 | |
| Rotational speed, rpm | 0 | | 0 | | 0 | | 0 | | 0 | |
| Heater symbol | Heat loss | | Heat loss | | Heat loss | | Heat loss | | Heat loss | |
| | Btu/(hr) (sq ft) | Percent (a) | Btu/(hr) (sq ft) | Percent (a) | Btu/(hr) (sq ft) | Percent (a) | Btu/(hr) (sq ft) | Percent (a) | Btu/(hr) (sq ft) | Percent (a) |
| A | 194 | 13.0 | 258 | 13.0 | 215 | 14.5 | 258 | 13.0 | 425 | 17.2 |
| B | 108 | 7.2 | 408 | 20.6 | 108 | 7.2 | 150 | 7.6 | 237 | 9.6 |
| C | 280 | 18.9 | 430 | 21.7 | [b]165 | [b]11.1 | 323 | 16.3 | 540 | 21.8 |
| D | 258 | 17.4 | 323 | 16.3 | 150 | 10.1 | 258 | 13.0 | 323 | 13.0 |
| E | 95 | 6.4 | 129 | 6.5 | [b]86 | [b]5.8 | [b]80 | [b]4.0 | [b]120 | [b]4.8 |
| F | 86 | 5.8 | 129 | 6.5 | 86 | 5.8 | [b]130 | [b]6.6 | 172 | 7.0 |

| Air velocity, mph | 175 | | 175 | | 175 | | 175 | | 275 | | 275 | |
|---|---|---|---|---|---|---|---|---|---|---|---|---|
| Power density, w/sq in. | 3 | | 4 | | 3 | | 4 | | 3 | | 4 | |
| Rotational speed, rpm | 800 | | 800 | | 1200 | | 1200 | | 1200 | | 1200 | |
| Heater symbol | Heat loss | | Heat loss | | Heat loss | | Heat loss | | Heat loss | | Heat loss | |
| | Btu/(hr) (sq ft) | Percent (a) | Btu/(hr) (sq ft) | Percent (a) | Btu/(hr) (sq ft) | Percent (a) | Btu/(hr) (sq ft) | Percent (a) | Btu/(hr) (sq ft) | Percent (a) | Btu/(hr) (sq ft) | Percent (a) |
| A | 150 | 10.1 | 236 | 11.9 | 172 | 11.6 | 237 | 12.0 | 158 | 10.6 | 237 | 12.0 |
| B | 108 | 7.3 | 193 | 9.7 | 107 | 7.2 | 193 | 9.8 | 131 | 8.8 | 150 | 7.6 |
| C | 323 | 21.7 | [b]420 | [b]21.2 | [b]325 | [b]21.9 | 387 | 19.5 | 116 | 7.8 | [b]275 | [b]13.9 |
| D | 150 | 10.1 | 220 | 11.1 | [b]130 | [b]8.8 | [b]210 | [b]10.6 | 92 | 6.2 | 301 | 15.2 |
| E | [b]130 | [b]8.8 | 200 | 10.1 | [b]125 | [b]8.4 | [b]140 | [b]7.1 | [b]70 | [b]4.7 | [b]130 | [b]6.6 |
| F | 160 | 10.8 | 240 | 12.1 | [b]140 | [b]9.4 | 215 | 10.8 | 89 | 6.0 | 215 | 10.9 |

[a]Percent of total heat input.

[b]Estimated.

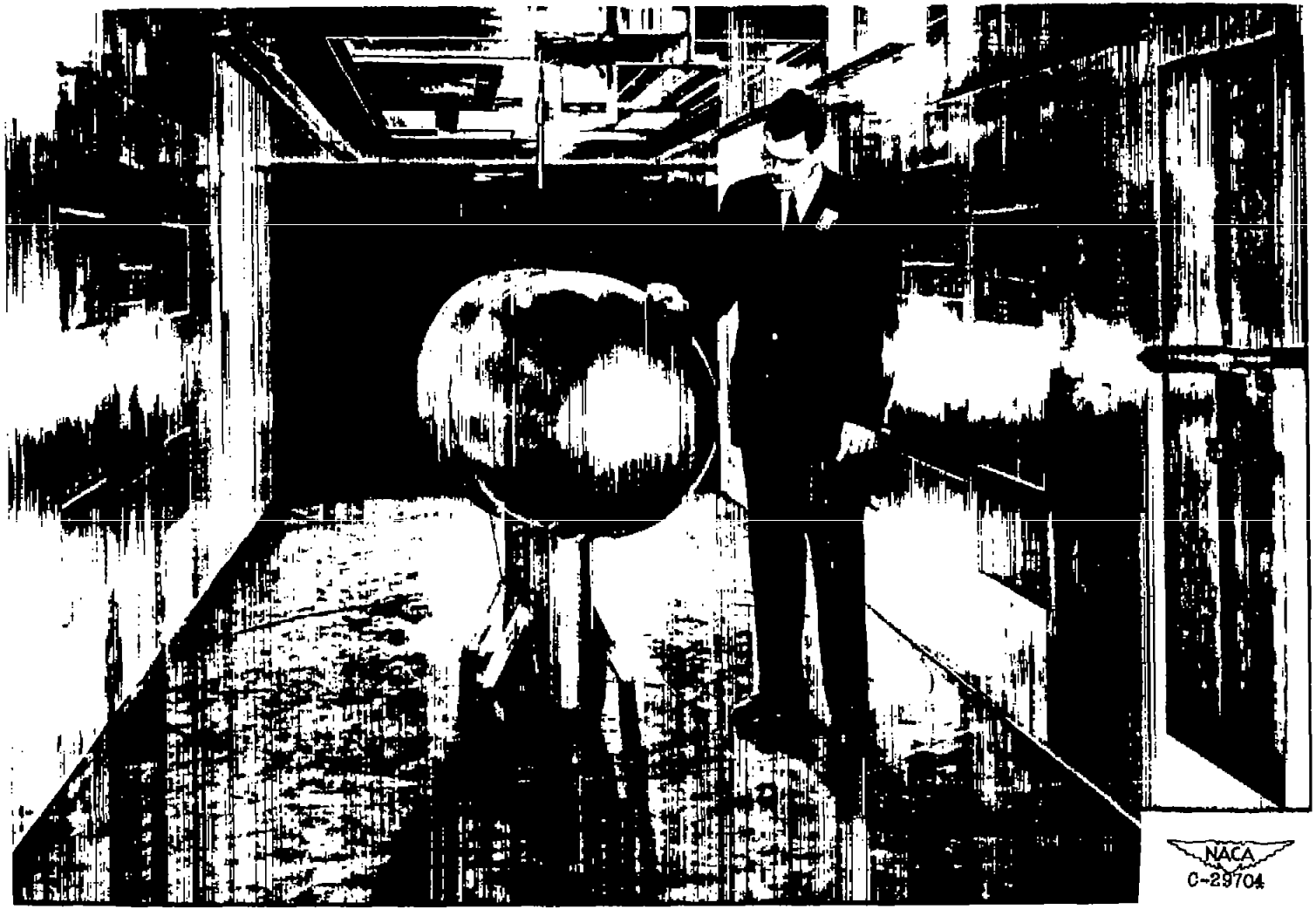


Figure 1. - Installation of heated spinner in test section of icing-research tunnel.

| Spinner coordinates | |
|---|---|
| Axial dimension, in. | Radial dimension, in. |
| 0 | 0 |
| .25 | 1.64 |
| .50 | 2.32 |
| 1.5 | 4.15 |
| 2.5 | 5.36 |
| 3.5 | 6.29 |
| 5.5 | 7.80 |
| 7.5 | 9.00 |
| 9.5 | 9.98 |
| 11.5 | 10.80 |
| 13.5 | 11.52 |
| 15.5 | 12.15 |
| 17.5 | 12.69 |
| 19.5 | 13.15 |
| 21.5 | 13.55 |
| 23.5 | 13.90 |
| 25.5 | 14.20 |
| 27.5 | 14.45 |
| 29.5 | 14.65 |
| 31.5 | 14.80 |
| 33.5 | 14.91 |
| 35.5 | 14.97 |
| 37.5 | 15.00 |

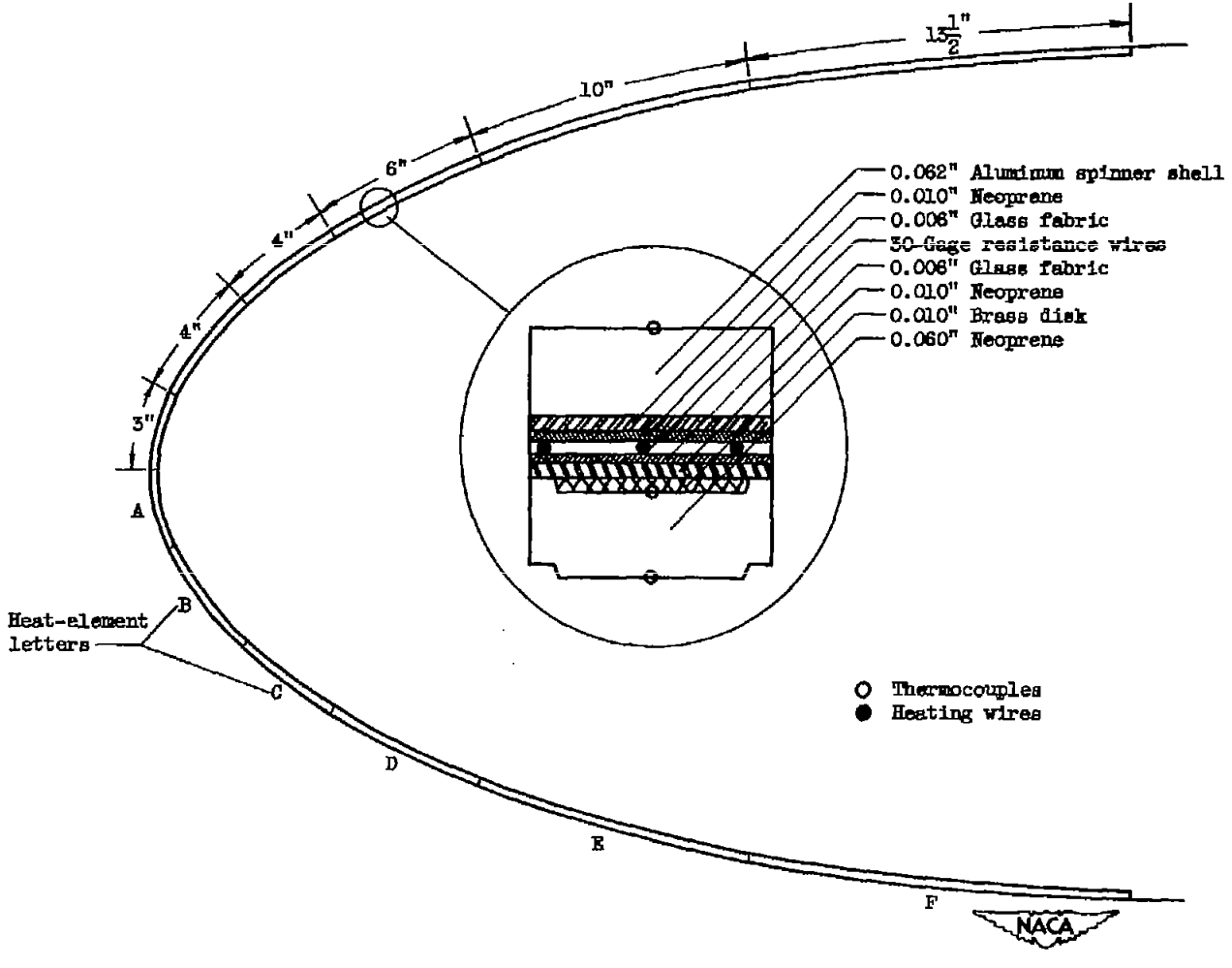


Figure 2. - Spinner contour and construction details of heater.

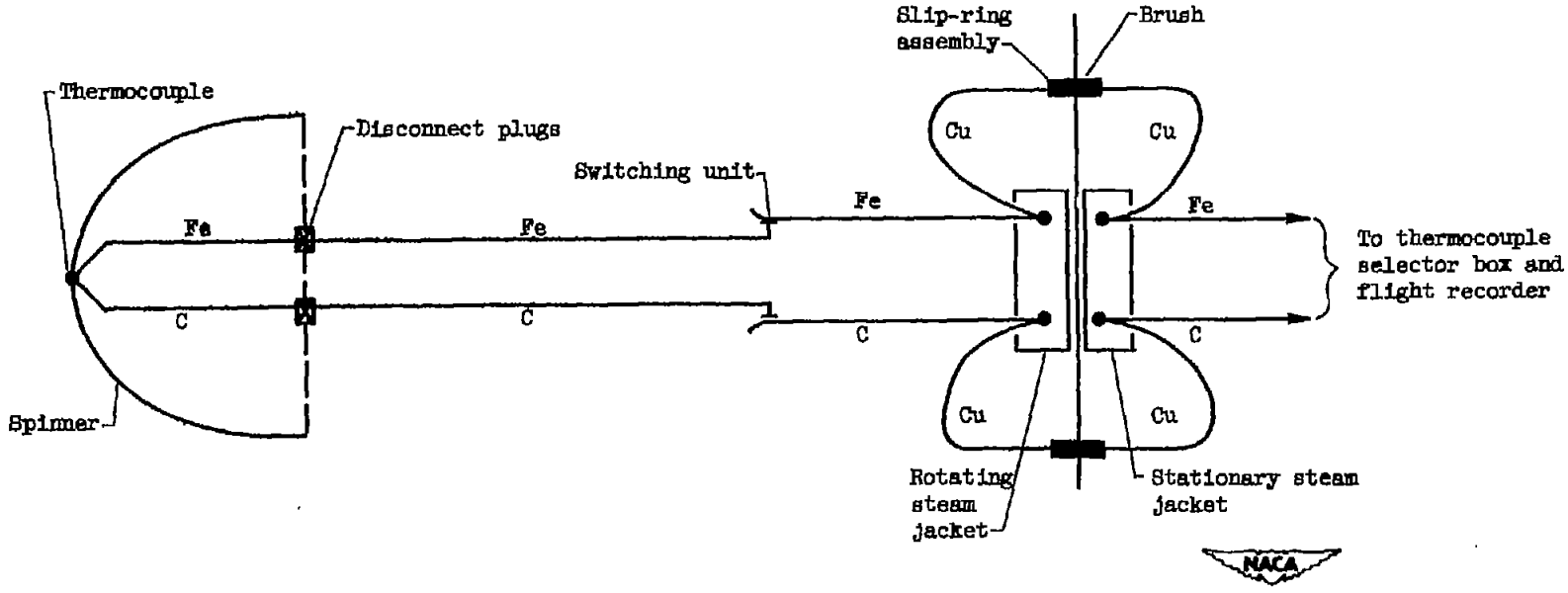


Figure 3. - Schematic diagram showing temperature-measuring system used for spinner. C, constantan; Fe, iron; Cu, copper.

2906

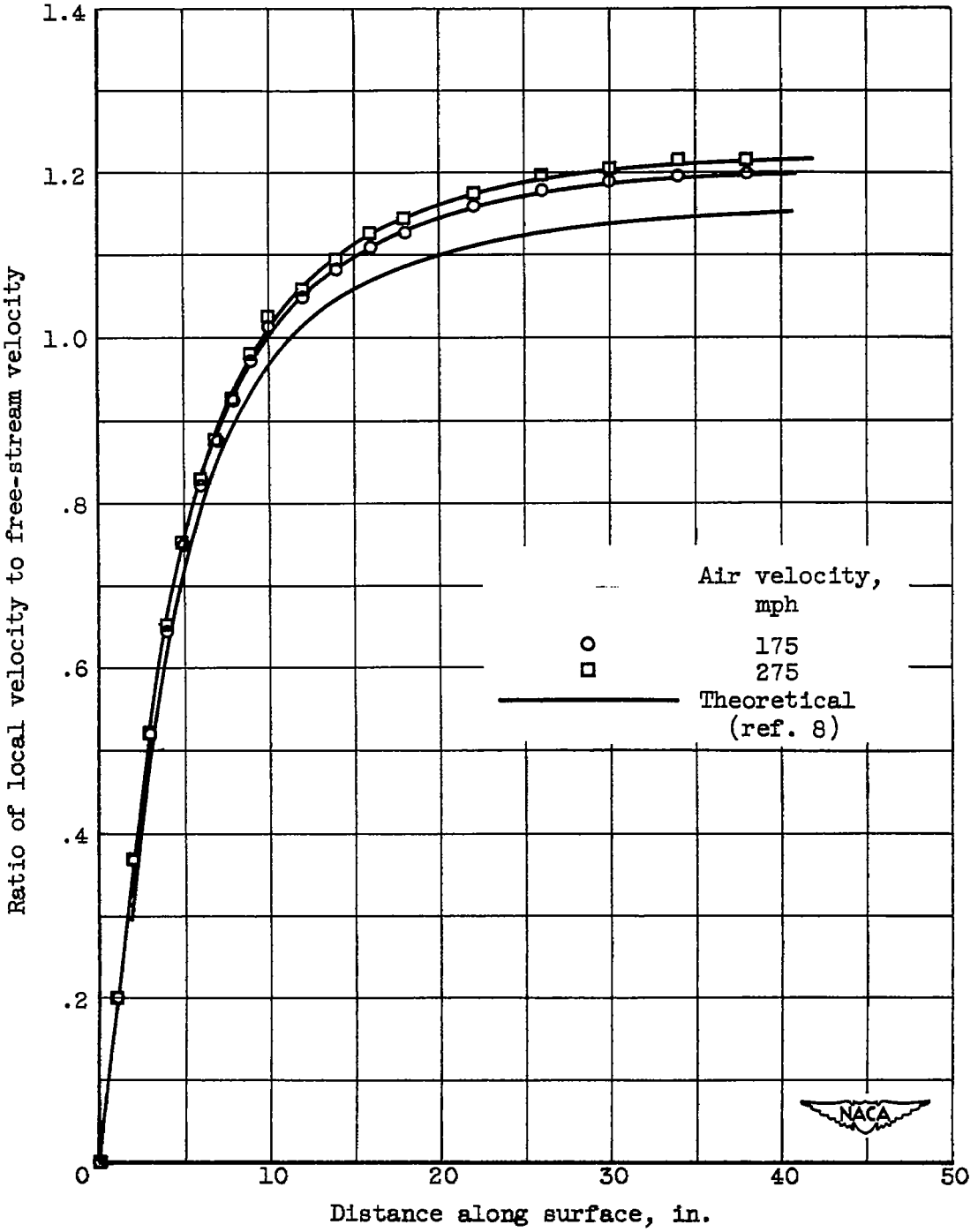


(a) Zero angle of attack.

Figure 4. - Velocity distribution over stationary spinner for angles of attack of zero and 4°.

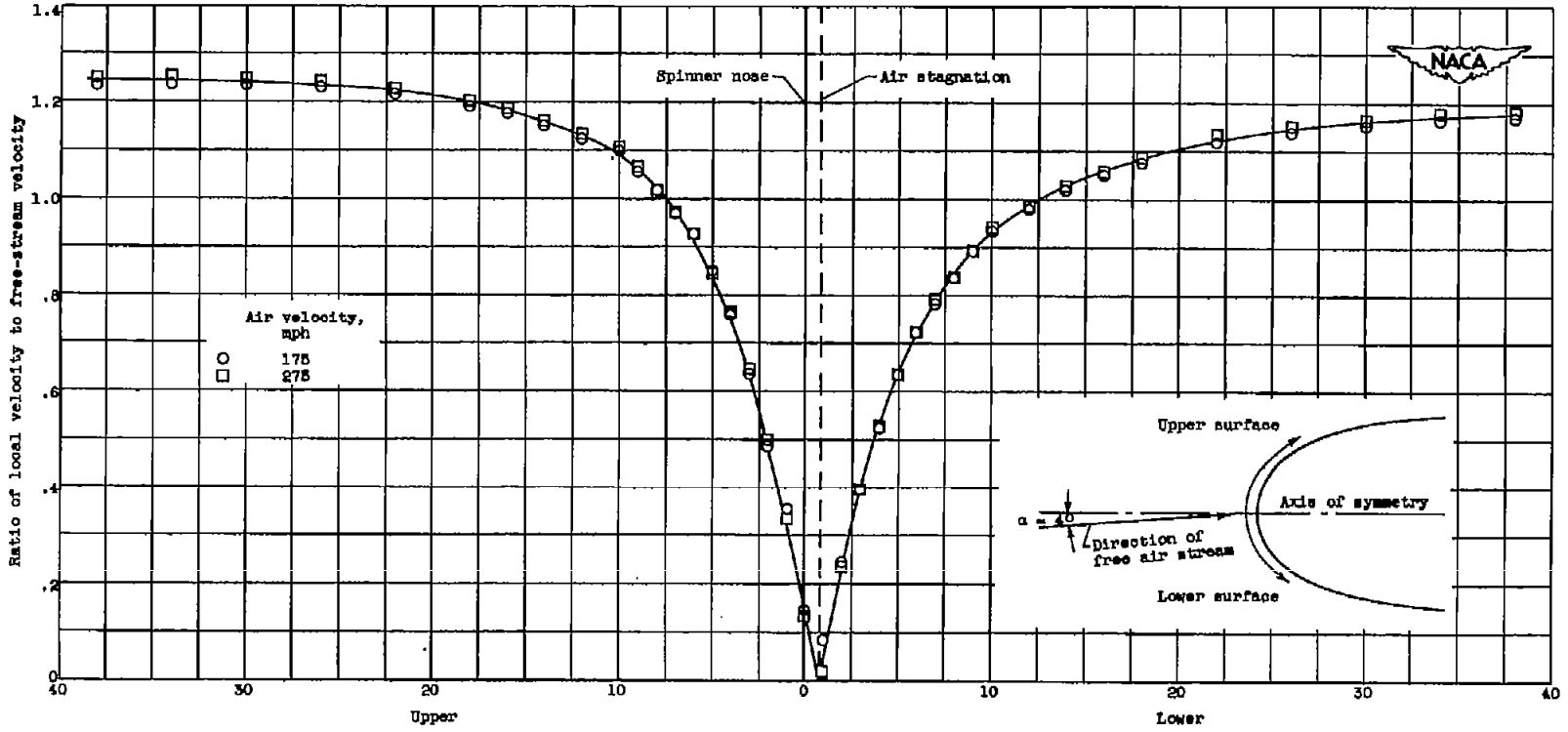


(b) Angles of attack, 4°.

Figure 4. - Concluded. Velocity distribution over stationary spinner for angles of attack of zero and 4°.

2906

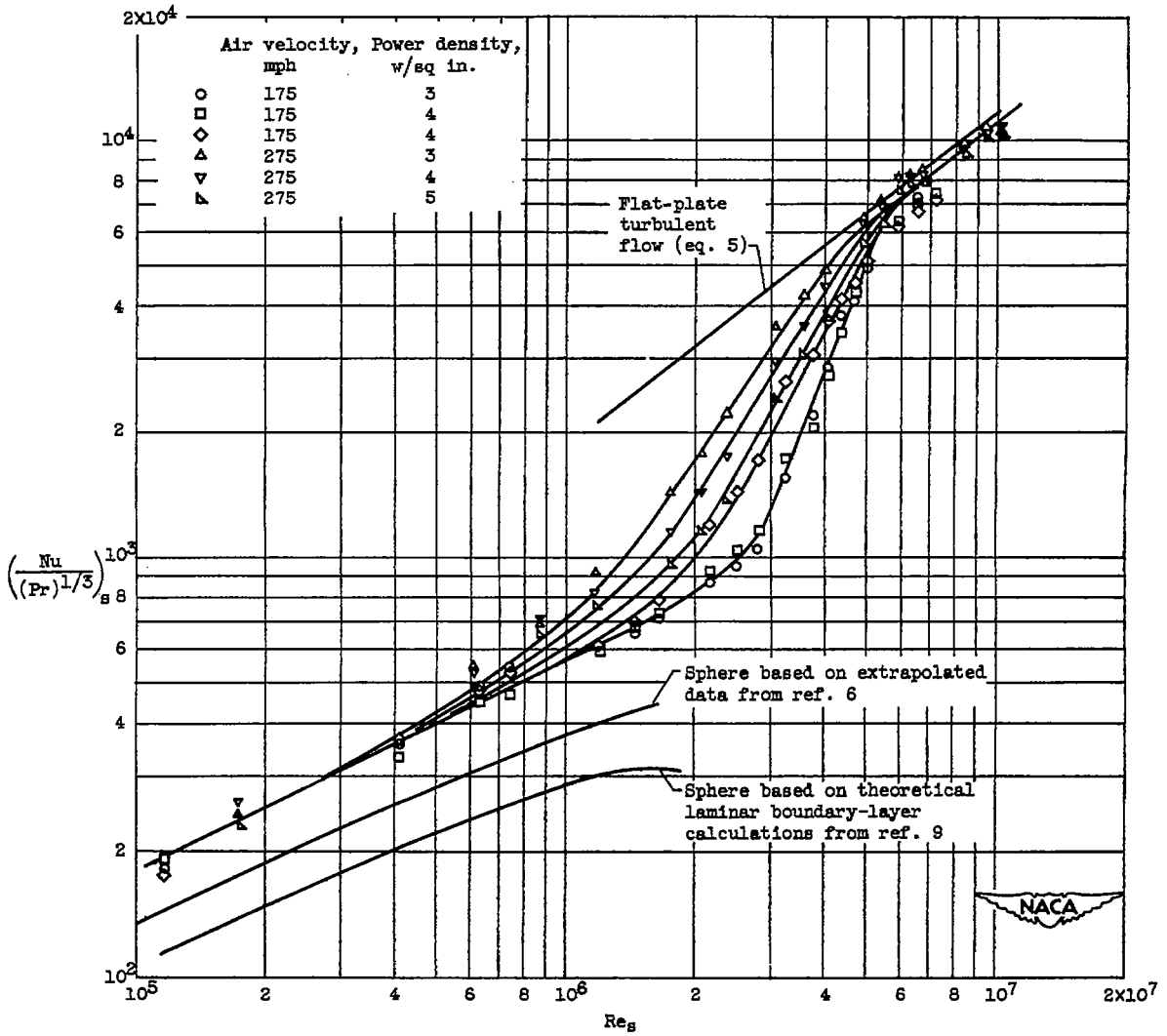


Figure 5. - Correlation of heat-transfer data obtained with uniform heating densities for stationary spinner. Zero angle of attack.

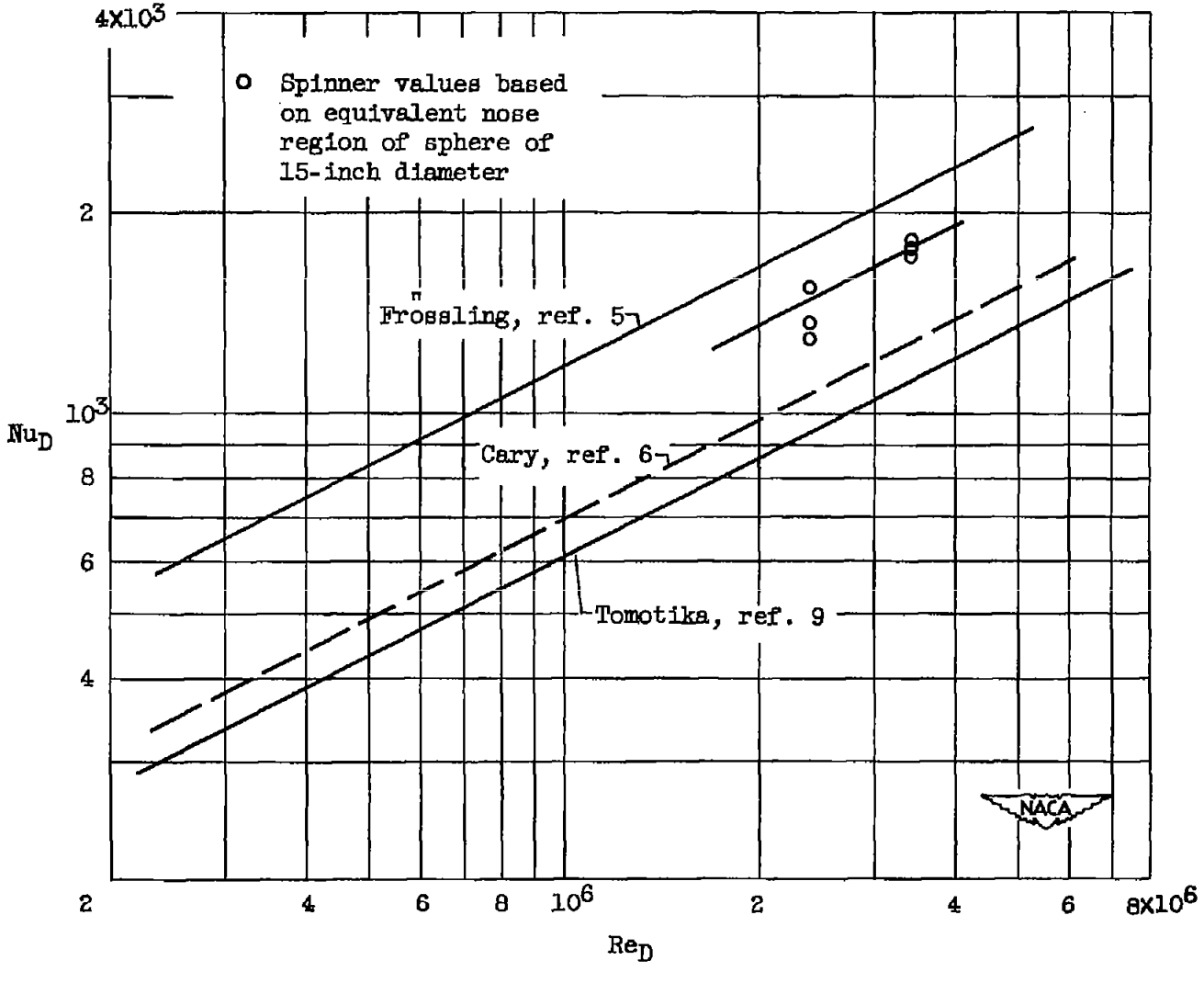


Figure 6. - Comparison of heat transfer from stagnation point of stationary spinner and sphere.

2906

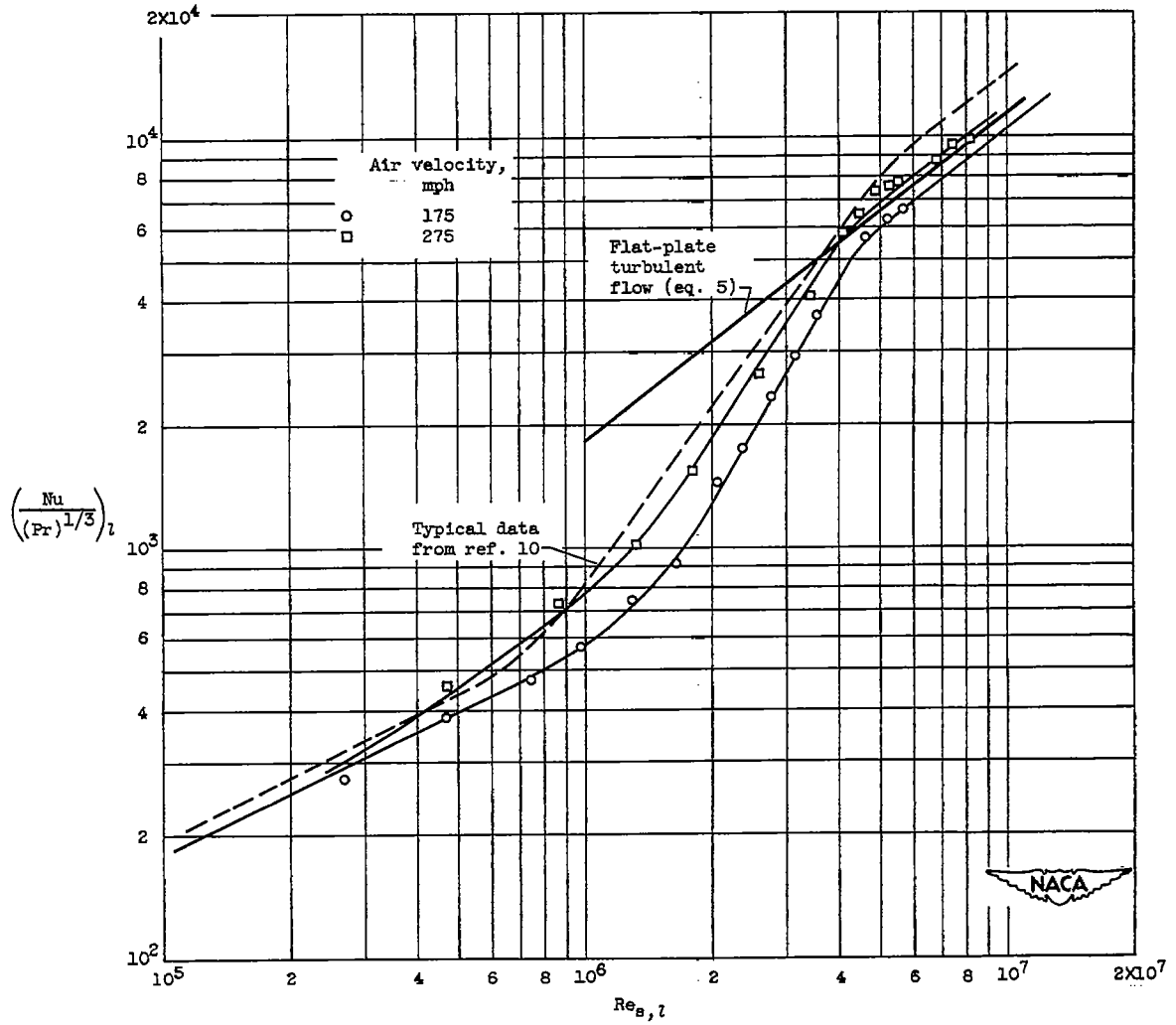


Figure 7. - Comparison of heat-transfer data based on local values of air viscosity, density, and thermal conductivity for stationary spinner with results from NACA 65,2-016 airfoil (ref. 10). Power density, 4 watts per square inch.

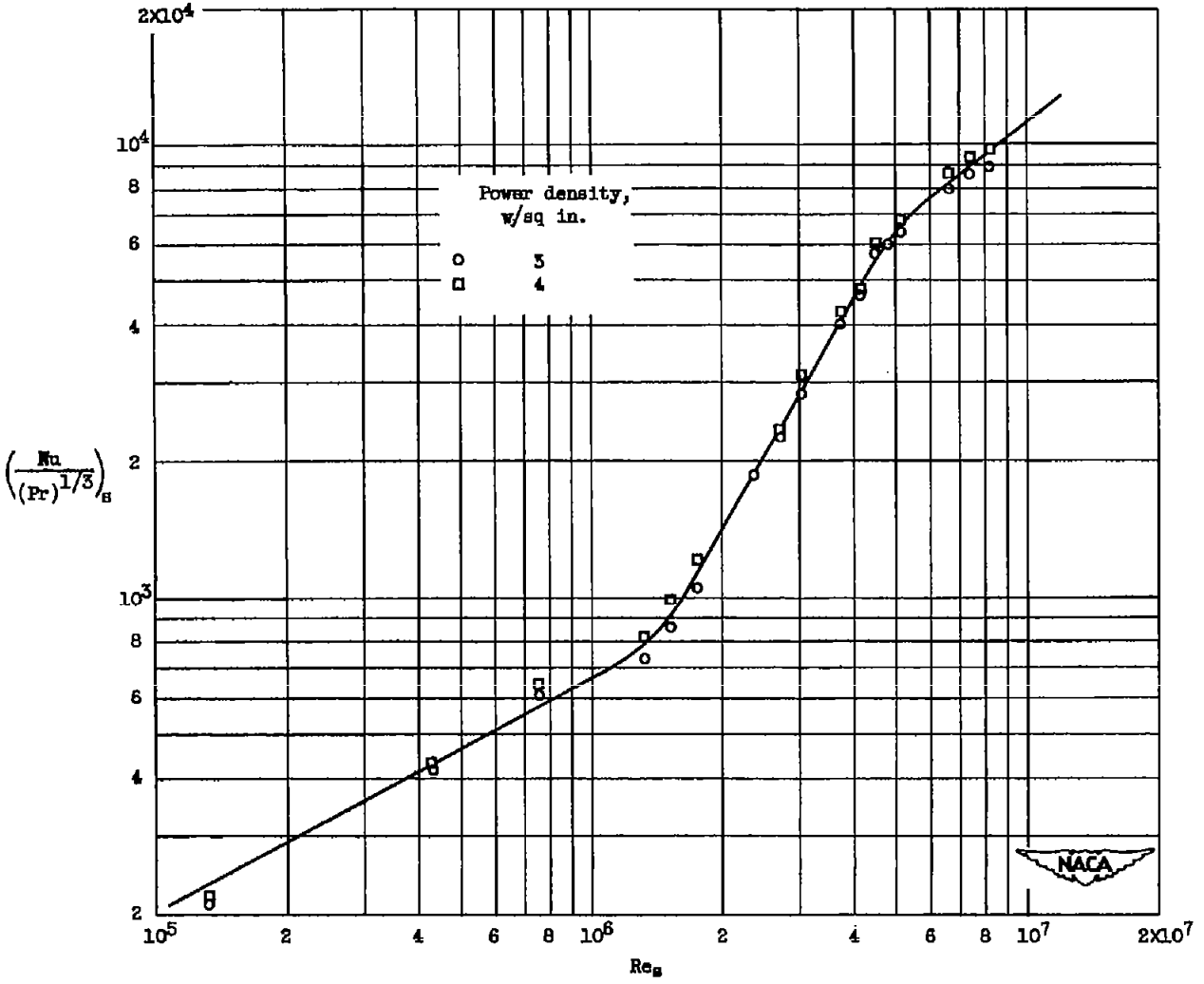


(a) Rotational speed, 800 rpm.

Figure 8. - Correlation of heat-transfer data obtained with uniform heating densities for rotating spinner. Zero angle of attack; air speed, 175 miles per hour.

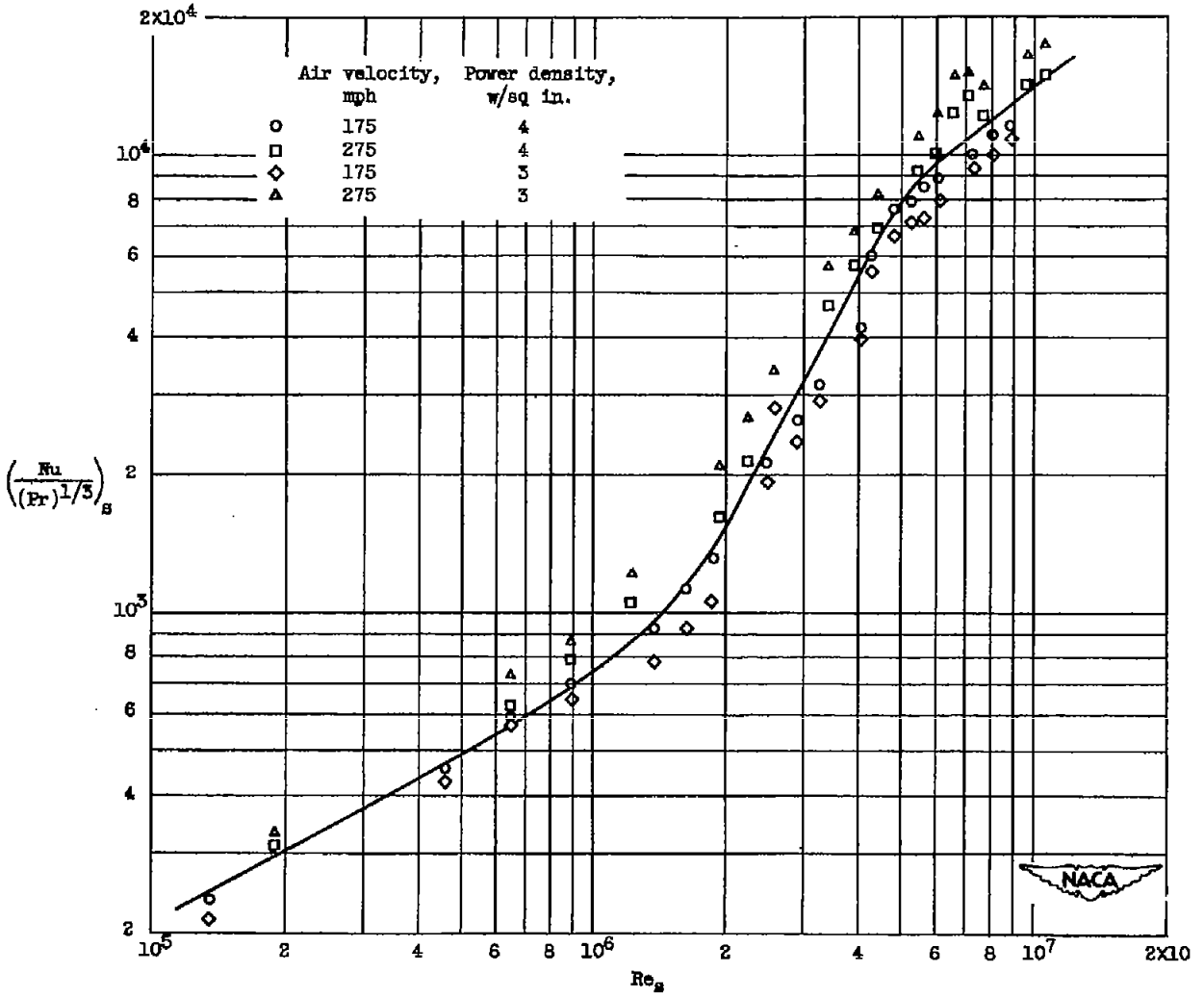


(b) Rotational speed, 1200 rpm.

Figure 8. - Concluded. Correlation of heat-transfer data obtained with uniform heating densities for rotating spinner. Zero angle of attack; air speed, 175 miles per hour.

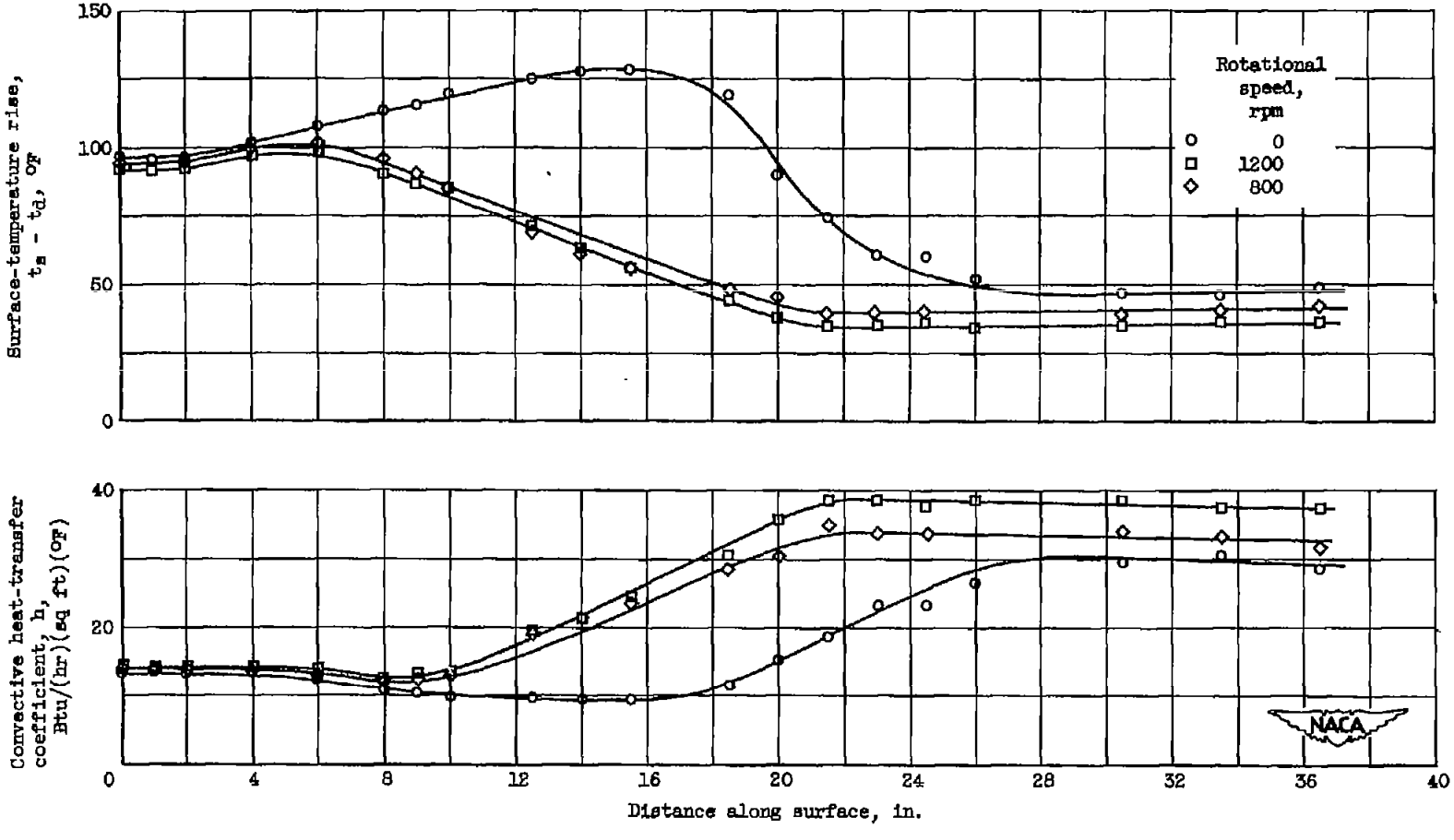


(a) Air velocity, 175 miles per hour; power density, 3 watts per square inch.

Figure 9. - Heat-transfer data obtained for both stationary and rotating operation of spinner with uniform heating rate. Zero angle of attack.

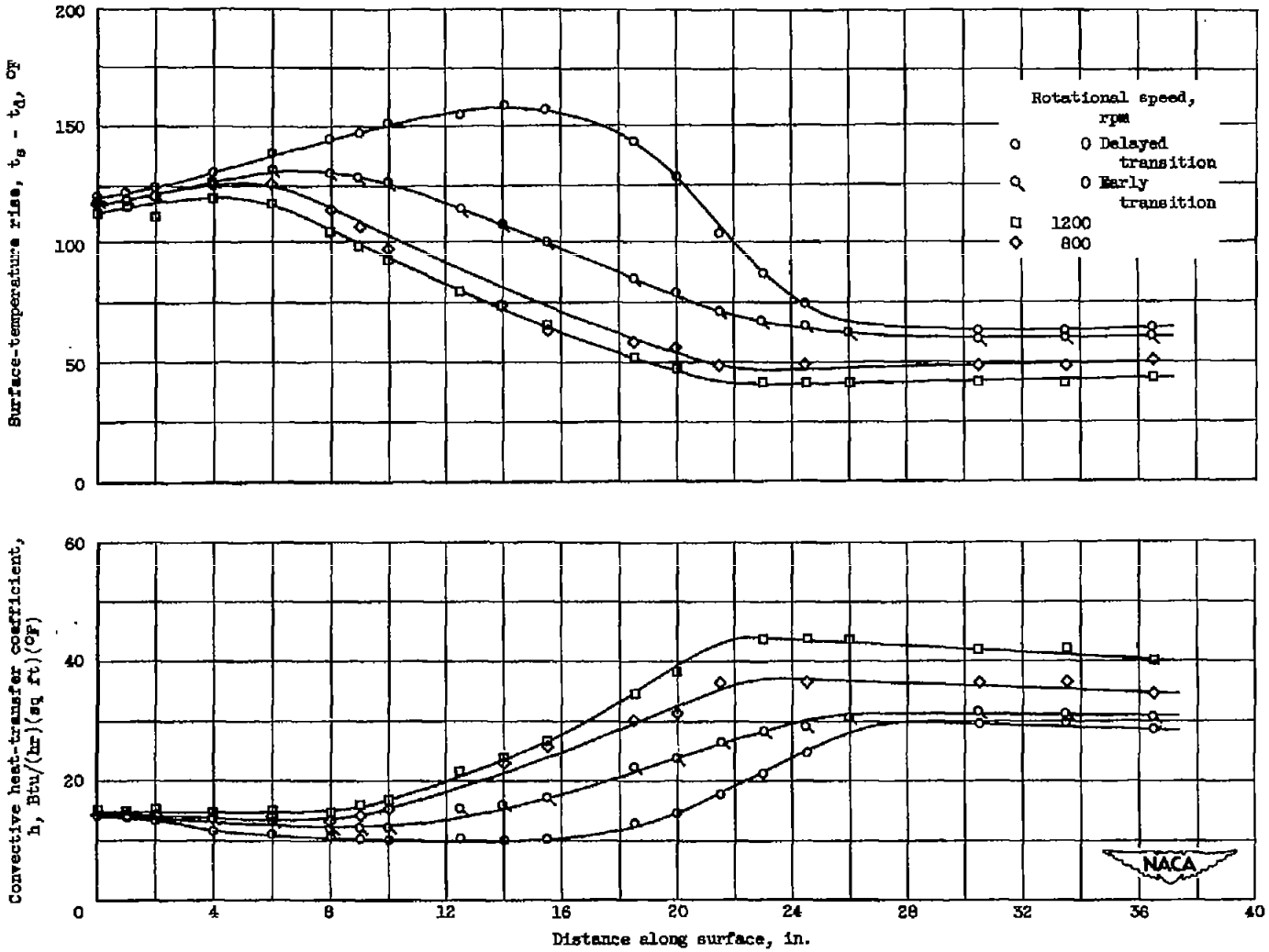


(b) Air velocity, 175 miles per hour; power density, 4 watts per square inch.

Figure 9. - Continued. Heat-transfer data obtained for both stationary and rotating operation of spinner with uniform heating rate. Zero angle of attack.

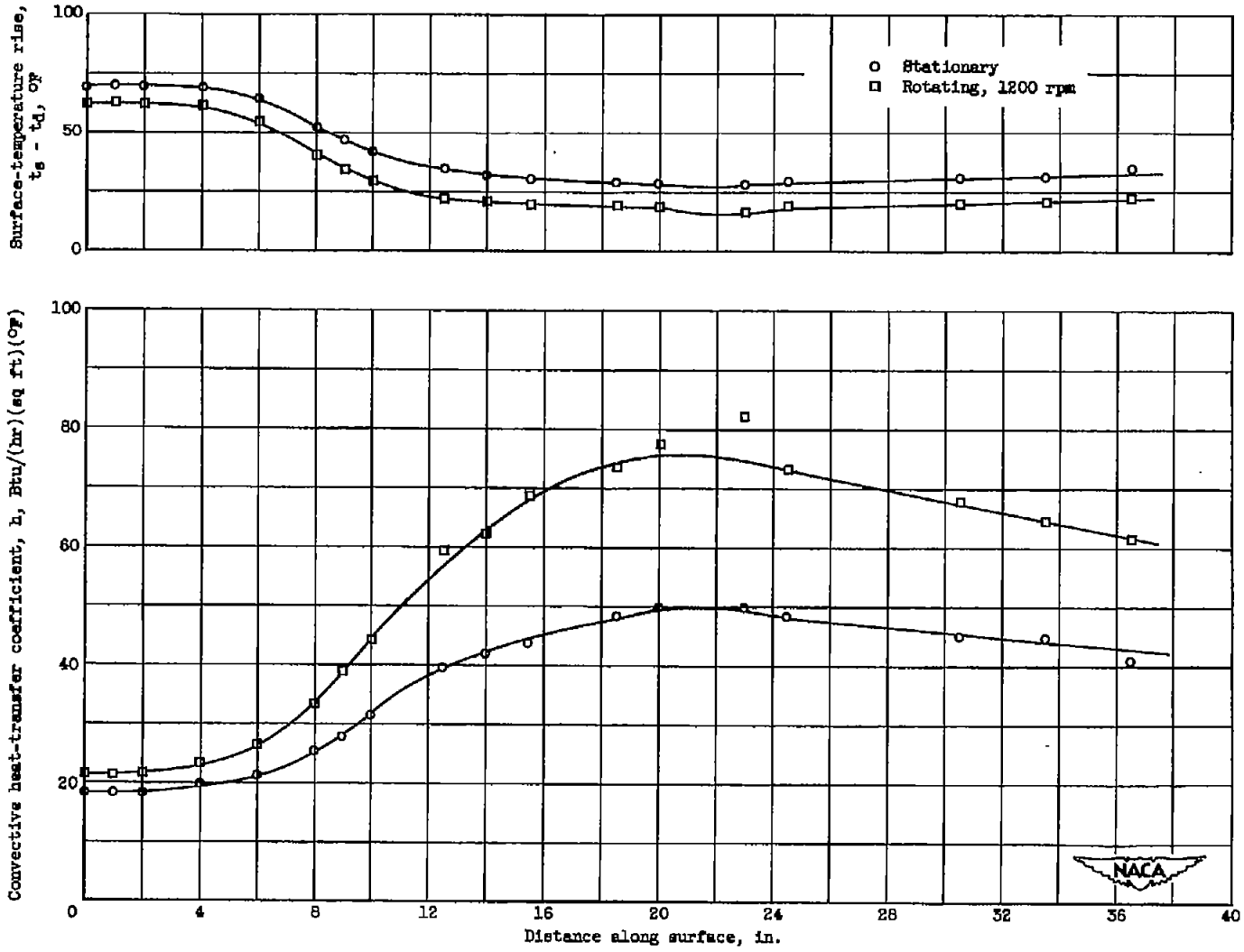


(c) Air velocity, 275 miles per hour; power density, 3 watts per square inch.

Figure 9. - Continued. Heat-transfer data obtained for both stationary and rotating operation of spinner with uniform heating rate. Zero angle of attack.

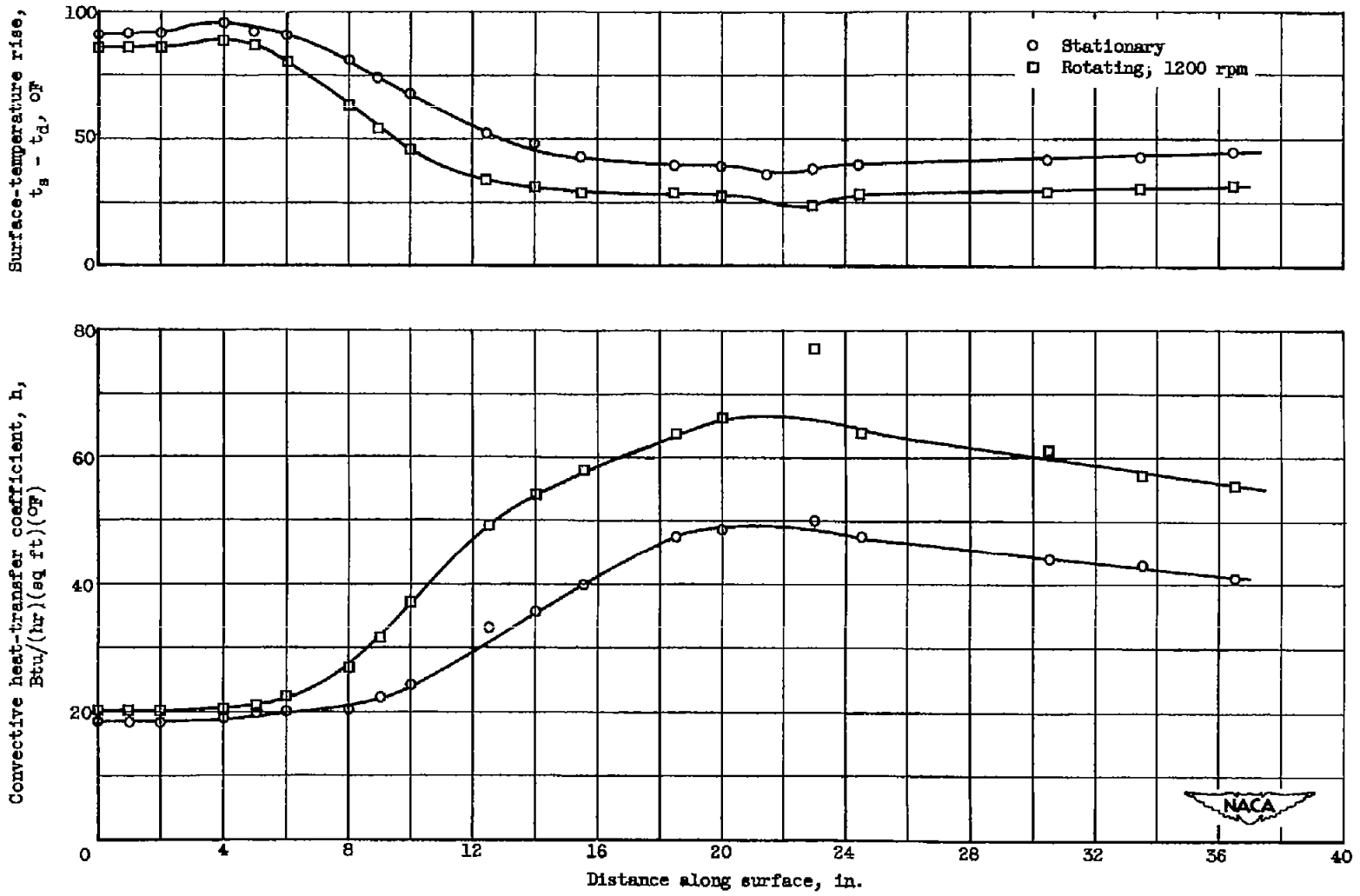


(d) Air velocity, 275 miles per hour; power density, 4 watts per square inch.

Figure 9. - Continued. Heat-transfer data obtained for both stationary and rotating operation of spinner with uniform heating rate. Zero angle of attack.

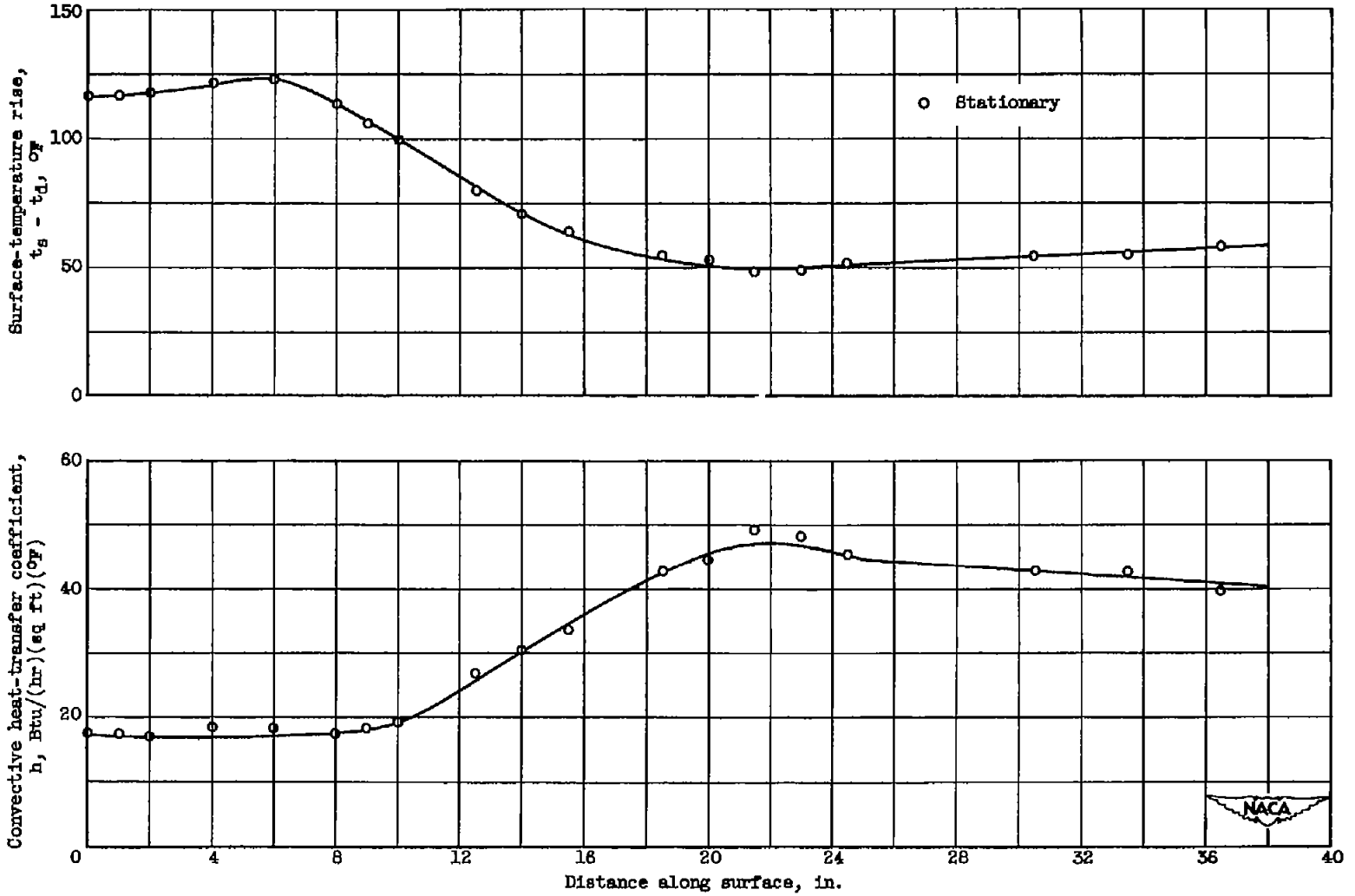


(e) Air velocity, 275 miles per hour; power density, 5 watts per square inch.

Figure 9. - Concluded. Heat-transfer data obtained for both stationary and rotating operation of spinner with uniform heating rate. Zero angle of attack.

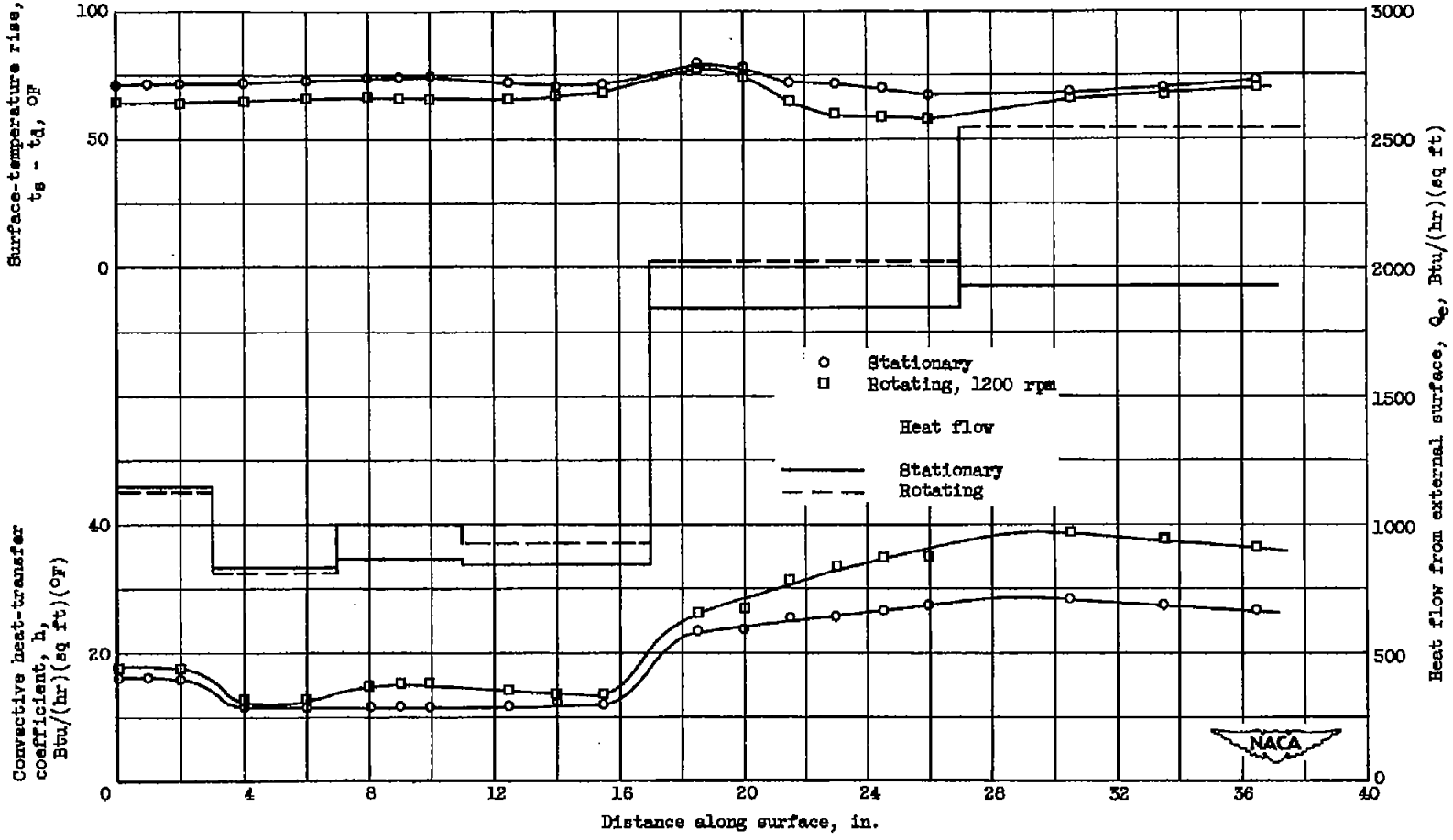


(a) Air velocity, 175 miles per hour.

Figure 10. - Heat-transfer data obtained from both stationary and rotating operation of spinner with uniform surface temperature and nonuniform heating rate. Zero angle of attack.

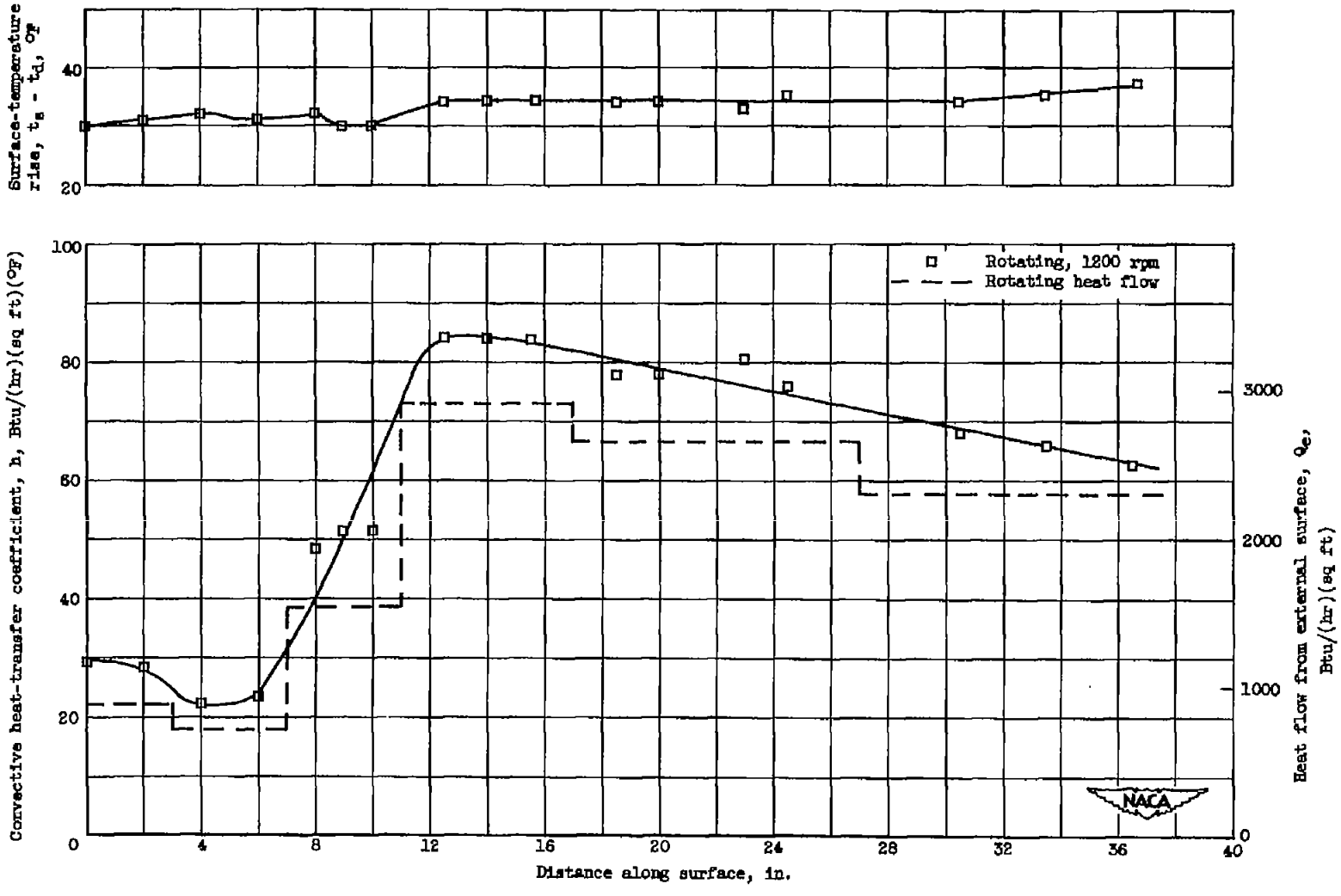


(b) Air velocity, 275 miles per hour.

Figure 10. - Concluded. Heat-transfer data obtained from both stationary and rotating operation of spinner with uniform surface temperature and nonuniform heating rates. Zero angle of attack.

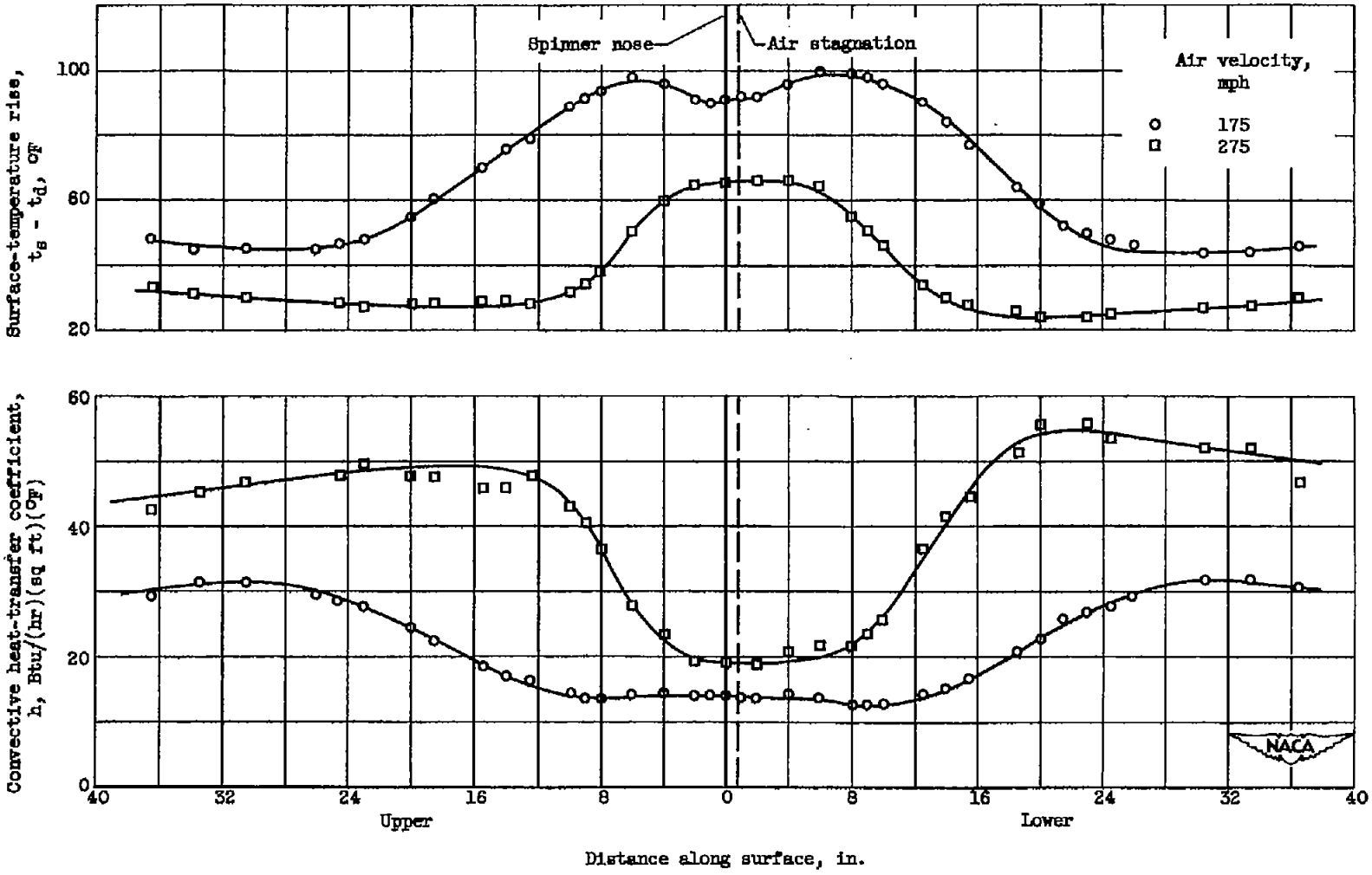


(a) Power density, 3 watts per square inch.

Figure 11. - Heat-transfer data obtained for stationary operation of spinner with uniform heating densities. Angle of attack, 4°.

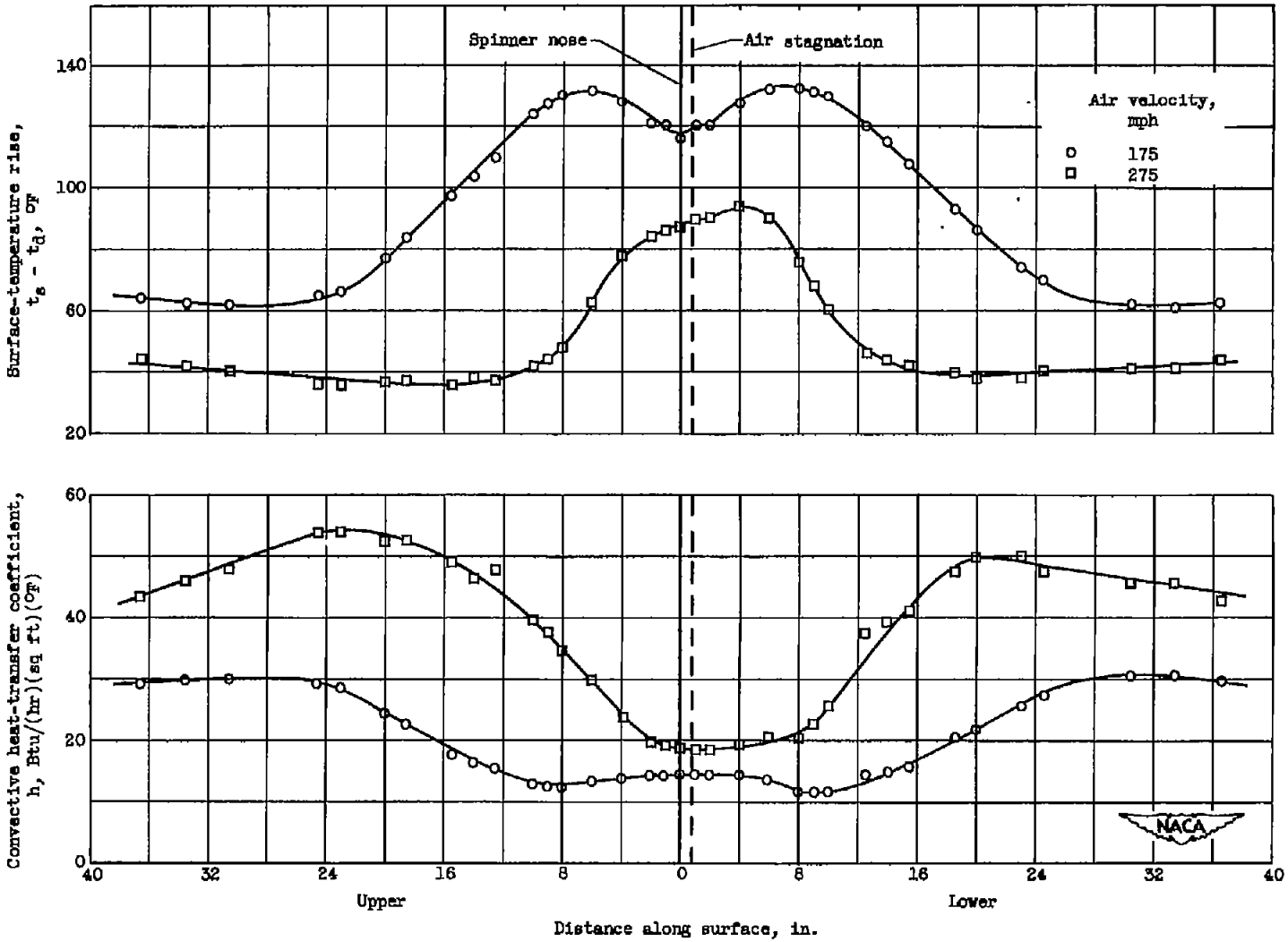


(b) Power density, 4 watts per square inch.

Figure 11. - Concluded. Heat-transfer data obtained for stationary operation of spinner with uniform heating densities. Angle of attack, 4°.



NACA-Langley - 8-6-53 - 425